

Antiresonant driven systems for particle manipulation

M. Florencia Carusela^{1,2,*}, Paolo Magaretti^{3,4,5,†} and J. Miguel Rubi^{6‡}

¹ *Instituto de Ciencias, Universidad Nacional de General Sarmiento, Los Polvorines, Buenos Aires, Argentina*

² *National Scientific and Technical Research Council, Argentina*

³ *Max Planck Institute for Intelligent Systems, Heisenbergstr. 3, 70569 Stuttgart, Germany*

⁴ *IV Institute for Theoretical Physics, University of Stuttgart, Pfaffenwaldring 57, 70569 Stuttgart, Germany*

⁵ *Helmholtz Institut Erlangen-Nürnberg for Renewable Energy (IEK-11),*

Forschungszentrum Jülich, Fürther Str. 248, 90429, Nürnberg, Germany and

⁶ *Departament de Física de la Materia Condensada, Universitat de Barcelona, Barcelona, Spain*

We report on the onset of anti-resonant behaviour of mass transport systems driven by time-dependent forces. Anti-resonances arise from the coupling of a sufficiently high number of space-time modes of the force. The presence of forces having a wide space-time spectrum, a necessary condition for the formation of an anti-resonance, is typical of confined systems with uneven and deformable walls that induce entropic forces dependent on space and time. We have analyzed, in particular, the case of polymer chains confined in a flexible channel and shown how they can be sorted and trapped. The presence of resonance-antiresonance pairs found can be exploited to design protocols able to engineer optimal transport processes and to manipulate the dynamics of nano-objects.

I. INTRODUCTION

Many biological processes and micro- and nano-technological applications depend on the dynamics of soft systems, such as electrolytes, polymers and macromolecules [1–5], which are confined. This is, for example, the case of ionic and microfluidic channels [6, 7], blue energy rectifiers [8] and DNA-sequencing devices [4]. Due to their small size, the dynamics of these systems are strongly affected by thermal noise and by noise generated by external sources.

The interplay between noise and external forces has been so far analyzed for cases in which only one or some few spatial and/or temporal modes contribute to the force. Indeed, in Brownian ratchets, although the force may consist of different spatial modes, its dependence on time typically reduces to a single mode [9–15]. In contrast, in ghost stochastic resonance [16] multiple temporal frequencies are involved in the force but just a single spatial modes is excited. So far, the most general situation in which the force spectrum includes harmonics of a higher order both in time and space has not been analyzed. Such a scenario can be realized by means of optical, electric or magnetic fields [17–19] or by forces resulting from the geometrical confinement of the particles. This is the case of the undulatory motion of worm-like organisms [20, 21], peristaltic pumping [22–25], fluctuating ion channels and pores [26–37] as well as synthetic soft micro- nanofluidic devices [38–40]. Knowing what the impact of higher order harmonics is on the response of the system is a question of great current interest.

In this Article, we show that when a greater number of space-time modes contributes to the force spectrum,

the particle current develops resonance-antiresonance pairs that increase or decrease the current and can therefore, by engineering the spectrum, set up optimal scenarios for the manipulation and transport of particles. The presence of antiresonances is detected from a perturbative analysis of the average particle current that progressively incorporates different modes into the force spectrum. The analytical predictions are supported by numerical solutions performed for the case of a single polymer chain confined in a channel whose walls undergo sustained oscillations. We show that if the amplitude of the oscillations of the effective force on the polymer is large enough, the current exhibits a rich Fourier spectrum, even for simple single-mode oscillations of the shape of the walls. Our numerical data confirm that the onset of the resonance-antiresonance pairs is controlled by the "richness" of the Fourier spectrum of the effective force acting on the polymer.

II. RESONANCE-ANTIRESONANCE PAIR FORMATION

In the overdamped regime, the evolution of the probability distribution $\rho(x, t)$ is governed by the Smoluchowski equation

$$\frac{\partial \rho(x, t)}{\partial t} = -\frac{\partial J(x, t)}{\partial x} = D \frac{\partial}{\partial x} \left[\frac{\partial}{\partial x} - \beta f(x, t) \right] \rho(x, t) \quad (1)$$

where D is the diffusion coefficient of the particle and $\beta^{-1} = k_B T$, with k_B the Boltzmann constant and T the absolute temperature. After relaxation of the initial conditions, the density and current averaged over time (over the period of the force) are no longer dependent on time and reach a stable value. In order to obtain an analytical view of the process, we assume that the local

* flor@campus.ungs.edu.ar

† p.malgaretti@fz-juelich.de

‡ mrubi@ub.edu

force can be decomposed as

$$f(x, t) = f_0 + f_1(x, t) \quad (2)$$

with f_0 a constant force. We expand both the time averaged density and flux for small values of f_1 (for a detailed derivation see Appendix IV). At first order, the time-averaged flux reads

$$J^{(1)} = 2 \sum_p \sum_v \bar{\rho} \beta^2 |f_{p,v}|^2 \frac{\beta \bar{f}_0}{k_v^2} \frac{\Gamma_{p,v} - 1}{\Gamma_{p,v}^2 + 4 \left(\frac{\beta \bar{f}_0}{k_v} \right)^2} \quad (3)$$

where $|f_{p,v}|$ is the amplitude of the Fourier mode of the force with frequency ω_p and wave number k_v and

$$\Gamma_{p,v} = \left(\frac{\omega_p}{Dk_v^2} \right)^2 + 1 - \left(\beta \frac{\bar{f}_0}{k_v} \right)^2 \quad (4)$$

is a function of the ratios between the three relevant time scales: the diffusion time $\sim 1/(Dk_v^2)$ for the mode with wavelength $2\pi/k_v$, the period of the force $\sim 1/\omega_p$ and the drift time $\sim 2\pi/(\beta D f_0 k_v)$. The second order contribution reads:

$$J^{(2)} = 2 \frac{\beta D}{L} \sum_p \sum_v \text{Re}(R_{p,v}^{(2)} f_{p,v}^*) \quad (5)$$

where $R_{p,v}^{(2)}$ are the amplitudes of the modes of the probability density at second order in the expansion (see Appendix IV).

$$R_{p,v}^{(2)} = - \frac{1}{\Gamma_{p,v} + 2\ell \frac{\beta \bar{f}_0}{k_v}} \sum_{n \neq p} \sum_i R_{n,i}^{(1)} \frac{\beta f_{p-n,v-i}}{k_v} \left[2\ell - \ell \frac{k_{v-i}}{k_v} \frac{k_{v-i} - 2k_i}{k_v} - 3 \left(\frac{\beta \bar{f}_0}{k_v} \right)^2 \right] \quad (6)$$

with

$$R_{n,i}^{(1)} = - \frac{\beta f_{n,i}}{k_i} \bar{\rho} \frac{\ell - \frac{\beta \bar{f}_0}{k_i}}{\Gamma_{n,i} + 2\ell \frac{\beta \bar{f}_0}{k_i}}. \quad (7)$$

For just one spatial or temporal mode, $R_{p,v}^{(2)}$ is zero since either $R_{p,v}^{(1)}$ or $f_{p,v}$ in Eq. (6) are zero and hence the contribution of $J^{(2)}$ to J becomes negligible. Accordingly, the total current is determined solely by its first order contribution $J^{(1)}$. Fig.1 shows that in this case J exhibits a resonant peak in agreement with previous studies on polymer translocation across fluctuating pores [26–29, 31]. When multiple spatial and temporal modes are present, $R_{p,v}^{(2)} \neq 0$ and hence $J^{(2)} \neq 0$. The coupling of these modes, not present in $J^{(1)}$, causes the formation of the resonant-antiresonant doublet of the current shown in Fig.1.

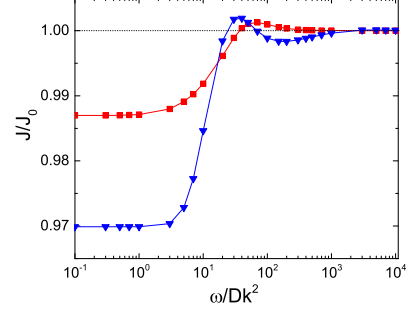


FIG. 1: Particle current J normalized to the current in a planar channel $J_0 = \beta D \rho_0 N f_0$ for $N_\omega = 9$ temporal modes and $N_k = 1, 12$ spatial modes corresponding respectively to red squares and blue downward triangles. ω and k denote respectively, the frequency and wave number of the oscillatory channel. Curves have been obtained for a force with $\text{Re}(f_{p,v}) = \frac{8}{5} \frac{1}{p}$ and $\text{Im}(f_{p,v}) = \frac{12}{5} (-1)^v \frac{1}{p}$.

III. RESONANCE-ANTIRESONANCE DOUBLETS FOR PARTICLE SORTING AND TRAPPING

A typical case in which the spatio-temporal spectrum of the external force induces an antiresonance is that of a nano-object moving in an environment bounded by irregular walls whose shape changes over time (Fig.2). In the case of a flexible pore, even though the deformation, characterized by its half-height, is given in terms of a single spatial and temporal mode

$$h(x, t) = h_0 + h_1 \cos(kx) \sin(\omega t) \quad (8)$$

the effective force induced on the confined particle is characterized by a rich Fourier spectrum. In order to show this, in the following we specialize the case of a Gaussian polymer chain confined in a 3D flexible channel whose half-height undergoes periodic oscillations according to Eq. (8).

When $h(x, t)$ varies smoothly ($|\partial_x h(x, t)| \ll 1$), the dynamics of the polymer can be mapped onto that of a point-like particle in the presence of the effective local free energy [41]

$$\beta \mathcal{F}(x, t) = -\beta N f_0 x + \beta A(x, t) \quad (9)$$

with

$$\begin{aligned} \beta A(x, t) &= \beta A_{cm}(x, t) + \beta A_{mon}(x, t) \quad (10) \\ &\equiv -2 \ln \left[\frac{16h(x, t)}{h_0 \pi^2} \right] - 2 \ln \left[\sum_{p=odd}^{\infty} \frac{e^{-\pi^2 p^2 \left(\frac{R_G}{2h(x, t)} \right)^2}}{p^2} \right] \end{aligned}$$

where $R_G = \sqrt{\frac{Nl^2}{6}}$ is the radius of gyration of the

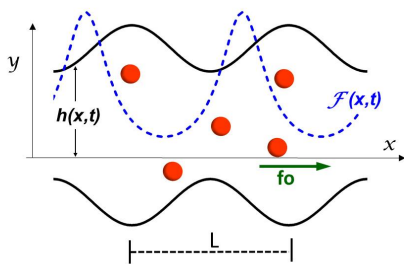


FIG. 2: Schematic representation of the Brownian motion of microscopic objects in an oscillatory channel of period L with a time-dependent radius $h(x,t)$ (in black). The free energy $\mathcal{F}(x,t)$ (in blue) consists of energetic and entropic contributions related to the applied force f_0 and to the entropic forces resulting from constrictions of the channel that give rise to a time- and space-dependent cross-sectional area.

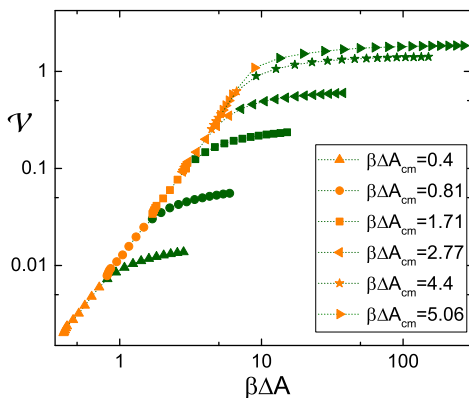


FIG. 3: Variance \mathcal{V} versus $\beta\Delta A$. Orange symbols correspond to the case $\Delta A_{mon}/\Delta A_{cm} < 1$ whereas green symbols to $\Delta A_{mon}/\Delta A_{cm} > 1$. Averages are taken during a time $T = 2\pi/\omega$.

polymer in an unbounded medium, N the number of monomers and r the Kuhn length. The first term on the rhs of Eq. (9) is an energetic contribution due to the action of external force f_0 on each monomer. The second term, denoted as $\beta A_{cm}(x,t)$, is an entropic contribution resulting from the number of allowed positions (microstates) of the centre of mass of the polymer within the channel [42–46] whereas the third one $\beta A_{mon}(x,t)$ accounts for the correction to the second term due to the presence of the other monomers [41]. The diffusion current J in Eq. (1) is obtained by considering that the force is $f(x,t) = -\frac{\partial \mathcal{F}(x,t)}{\partial x}$ and that, according to the Rouse model, $D = D_0/N$ is the diffusion coefficient of the polymer with D_0 that of a single monomer.

We remark the fact that even in the present case in which channel oscillations consist of a single k - ω mode, the spectrum of the force $f(x,t)$ contains

contributions from higher order spatial and temporal modes whose amplitudes depend on the maximum free energy difference

$$\beta\Delta A = \max_{x,t} \beta A(x,t) - \min_{x,t} \beta A(x,t). \quad (11)$$

For $\beta\Delta A \neq 0$, the amplitude of the modes is sensitive to the nature of the system. For confined hard spheres, A_{mon} drops out and the value of ΔA is controlled only by the geometry of the channel. Typical experimental realizations limits this value to $\beta\Delta A \lesssim 3$ [47]. For confined uncharged polymers, A_{mon} can give rise to arbitrary large values of ΔA upon increasing the radius of gyration R_G . Finally, for charged colloids, polymers or even more complex particles the magnitude of ΔA can be quite large [45, 48] and is controlled by both geometry of the channels and (electrostatic) interactions with the channel walls.

Our analysis reveals that the key factor for the onset of an antiresonance is the existence of a "rich" spectrum of both spatial and temporal modes of the external force. The "spectral richness" of the power spectrum $\mathcal{P}_{p,v} = f_{p,v}^2$ of a given external force $f(x,t)$ is captured by means of the variance

$$\mathcal{V} \equiv \langle \mathcal{P}_{p,v}^2 \rangle - \langle \mathcal{P}_{p,v} \rangle^2 \quad (12)$$

where $\langle \dots \rangle$ denotes average over p and v . Fig.3 shows \mathcal{V} versus $\beta\Delta A$, for different values of $\beta\Delta A_{cm}$ and $\beta\Delta A_{mon}$. For a given ΔA and $\Delta A_{mon}/\Delta A_{cm} < 1$, the variance displays a power law behavior represented by the orange master branch: $\mathcal{V} \approx (\beta\Delta A)^2$. For $\Delta A_{mon}/\Delta A_{cm} > 1$, it shows a significant sensitivity to changes of the parameters that characterize the channel geometry and the polymer, as evidenced by the appearance of multiple secondary branches (green symbols). On the other hand, given a value of ΔA_{cm} and varying ΔA along the master branch towards the corresponding secondary branch, the variance increases.

The presence of higher order harmonics of the force originates the antiresonance in the particle current J , normalized to the current for a flat channel J_0 , plotted in Fig.4-a. The different colors stand for the upward series of values $\beta\Delta A$ at which \mathcal{V} grows. In all cases, resonant/antiresonant maximum/minimum emerge with more pronounced minima at higher values of \mathcal{V} . Fig.4-a also shows the presence of different transport regimes. The limit $\omega/Dk^2 \rightarrow 0$ corresponds to the dynamics of a point-like particle moving in an almost static effective potential characterized by a free energy barrier $\beta\Delta A$ and under the action of an external force f_0 . In contrast, for $\omega/Dk^2 \rightarrow \infty$ the walls of the channel oscillate so fast, as compared to the typical time scale of the polymer, that it experiences an average potential equivalent to that of a polymer moving through a flat channel under the action of the external force f_0 [49]. In between these two limiting regimes, the current shows a non-monotonic behavior with a resonance and an antiresonance. In

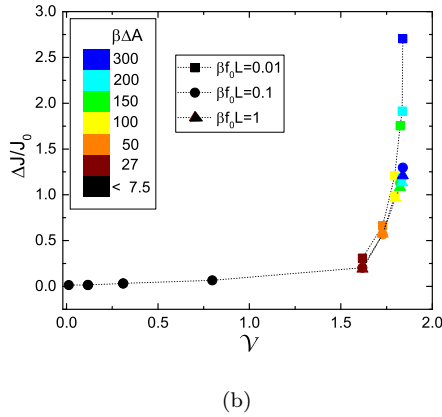
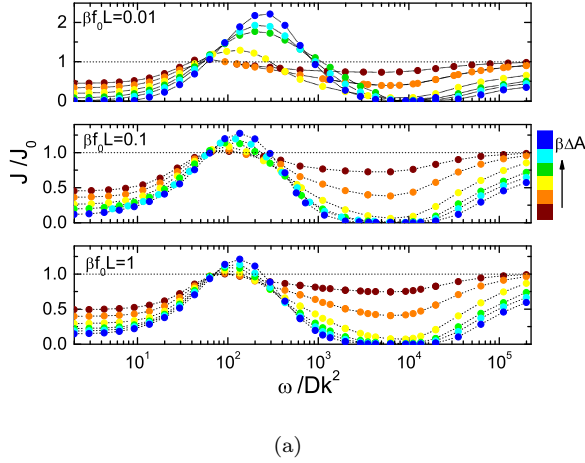


FIG. 4: (a): J/J_0 as a function of $\omega/(Dk^2)$ for $\beta f_0 L = 0.01, 0.1, 1$, $R_G = 0.03$, $N = 10$ and $\beta \Delta A_{cm} \approx 5$. Different colors correspond to increasing values (from brown to blue) of $\beta \Delta A = 27, 50, 100, 150, 200, 300$. The reference current is $J_0 = \beta D \rho_0 N f_0$, the current in the case of point particles moving through a flat channel. (b): $\Delta J/J_0$ (See Eq. (13)) versus \mathcal{V} for different values of the force and $\beta \Delta A$ (see legend).

particular, for all values of $\beta \Delta A$, J exhibits a resonant peak at $\frac{\omega}{Dk^2} \simeq 100$, as predicted by our model (see Eq. (3)). Interestingly, although the analytical results are obtained via a perturbative approach, the prediction about the appearance of a resonant peak is robust for high barriers and its location depends only weakly on the magnitude of $\beta \Delta A$. However, its amplification for increasing values of $\beta \Delta A$ is not found under this approach. The analytical results also predict the appearance of the antiresonance observed in Fig.4a). The onset of the antiresonance minimum is captured by the quantity

$$\Delta J \equiv J\left(\frac{\omega}{Dk^2} = 10^2\right) - J\left(\frac{\omega}{Dk^2} = 10^4\right) \quad (13)$$

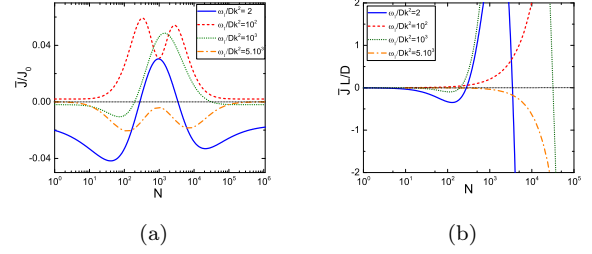


FIG. 5: (a) \bar{J}/J_0 and (b) $\bar{J}L/D$ versus N for the proposed protocol. $\omega_1 = 2$ (full), $\omega_1 = 10^2$ (dashed), $\omega_1 = 10^3$ (dotted), $\omega_1 = 5 \cdot 10^3$ (dotted-dashed) and $\omega_1 = 3 \cdot 10^4$ in all cases. Other parameters: $\beta \Delta A_{cm} = 5$, $\beta f_0 L = 0.1$, $b/h_0 = 0.01$.

Indeed, in the absence of an antiresonant minimum $\Delta J/J_0 \ll 1$, whereas once the antiresonance sets $\Delta J/J_0 \gtrsim 1$. Fig.4b shows that for a "simple" Fourier spectra ($\mathcal{V} < 1.5$) $\Delta J/J_0 \ll 1$, whereas for larger values of \mathcal{V} i.e. for a "rich" Fourier spectra $\Delta J/J_0 \gtrsim 1$ which triggers the antiresonance. The presence of a resonance-antiresonance doublet can be exploited to design a dynamical protocol able to sort and trap polymers. The protocol runs as follows: an external force f_0 is applied along with a time modulation of the channel half-height $h(x, t)$ characterized by a frequency ω_1 during a time $T/2$. Then the force is switched to $-f_0$ and the frequency to ω_2 . It is also applied during a time $T/2$. The time T is chosen such that $T \gg 2\pi/\omega_{1,2}$. Finally, we calculate the mean current in T

$$\bar{J} = \frac{J_1 + J_2}{2}, \quad (14)$$

where J_i are the average currents in each half-period computed as indicated previously.

Fig.5a, shows \bar{J} as function of N . We observe that chains with lengths in the range 10^2 to 10^4 times a monomer size can be immobilized and separated with a good resolution. The choice of $\omega_{1,2}$ is crucial to improve the performance of the protocol that requires the presence of a deep antiresonant minima that occur for large values of \mathcal{V} . Optimal conditions are achieved when one of the frequencies, say ω_2 , is the antiresonant one (Fig.5a). The protocol is particularly effective for long polymers, for which \bar{J} crosses the zero value with a very steep profile (see Fig.5b), with a value much larger than the characteristic diffusion velocity D/L . These conditions essentially take place when ω_1 is out of the amplification regime (resonance). For polymers whose lengths are very similar to that of the target (polymer with $\bar{J} = 0$), the signal-to-noise ratio is small which gives rise to a poor trapping resolution.

IV. CONCLUSIONS

In this article, we have shown that cooperation between the noise and an external forces whose spectrum contains a high enough number of harmonics leads to the appearance of new resonant states of the system. The occurrence of the resonant peak results from the well-known synchronisation of the hopping events induced by noise with the oscillations of the force (in our case of entropic origin). The increase in the number of modes of the force causes the system to move from a regime of a single resonant peak, typical of the case of a small number of modes, to a regime in which a pair of resonant-antiresonant peaks arises. The presence of a large number of modes causes the noise to synchronise with the different modes, which can lead to destructive interferences that make the particle current to decrease. Forces whose spectrum consists of a high number of coupled modes required for the appearance of antiresonances arise naturally in the case of systems confined by uneven and flexible walls.

We have shown this feature by analyzing the dynamics of a polymer chain confined within a channel whose walls undergo sustained oscillations. Our numerical data confirm the predictions of the analytical model and show a clear correlation between the number of modes (encoded in the variance of the Fourier power spectrum \mathcal{V}) and the onset of the antiresonant minimum.

The results obtained broaden the understanding of the resonant phenomena in drift-diffusion systems and may provide the rational for the interpretation of dataset existing in the literature [18, 37, 50, 51]. The existence of the new regimes we have found, in which resonances and antiresonances coexist, opens up the possibility of designing the driving force to be able to control the flow of particles and to manipulate nano-objects in order to study their properties.

M.F.C. thanks PIO-CONICET and PICT 18/2036, J.M.R. wants to thank financial support of MICIU of the Spanish Government, under Grant No. PGC2018-098373-B-I00.

APPENDIX

Our starting point is the 1D advection-diffusion equation:

$$\dot{\rho}(x, t) = \partial_x [D\partial_x \rho(x, t) - D\beta\rho(x, t)f(x, t)] \quad (15)$$

where $f(x, t)$ is the effective force acting on the point-like particle (for conservative forces we have $f(x, t) = -\partial_x W(x, t)$). We are interested in the long-time regime in which $\rho(x, t)$ can be assumed to be periodic in time.

Accordingly, we represent both ρ and f as:

$$\rho(x, t) = \sum_{n=-\infty}^{\infty} \rho_n(x) e^{i\omega_n t} \quad (16a)$$

$$\Rightarrow \rho_n(x) = \frac{1}{2\pi} \int \rho(x, t) e^{-i\omega_n t} dt \quad (16b)$$

$$f(x, t) = \sum_{n=-\infty}^{\infty} f_n(x) e^{i\omega_n t} \quad (16c)$$

$$\Rightarrow f_n(x) = \frac{1}{2\pi} \int f(x, t) e^{-i\omega_n t} dt \quad (16d)$$

The real nature of both ρ and f imposes the constraints on the amplitudes of the modes:

$$\text{Re}(\rho_n) = \text{Re}(\rho_{-n}) \quad (17a)$$

$$\text{Im}(\rho_n) = -\text{Im}(\rho_{-n}) \quad (17b)$$

$$\text{Re}(f_n) = \text{Re}(f_{-n}) \quad (17c)$$

$$\text{Im}(f_n) = -\text{Im}(f_{-n}) \quad (17d)$$

Using Eqs. (16), Eq. (15) one obtains

$$\begin{aligned} \sum_{n=-\infty}^{\infty} i\omega_n \rho_n(x) e^{i\omega_n t} = \\ \sum_{n,n=-\infty}^{\infty} \partial_x [D\partial_x \rho_n(x) - D\beta\rho_n(x)f_m(x)e^{i\omega_m t}] e^{i\omega_n t} \end{aligned} \quad (18)$$

Multiplying both sides of Eq.(18) by $e^{-i\omega_p t}$ and integrating in t we obtain:

$$i\omega_p \rho_p(x) = D\partial_x \left[\partial_x \rho_p(x) - \sum_{n=-\infty}^{\infty} \beta\rho_n(x)f_{p-n}(x) \right] \quad (19)$$

We assume periodic boundary conditions:

$$\rho(0, t) = \rho(L, t) \quad (20)$$

and use mass conservation

$$\int_0^L \rho(x, t) dx = L\bar{\rho}, \quad \forall t \quad (21)$$

In Fourier representation these equations leads to

$$\rho_0(0) = \rho_0(L) \quad (22)$$

and

$$\rho_n(0) = \rho_n(L) \quad (23)$$

Since mass conservation holds at all times, we have

$$\int_0^L \rho_0(x) dx = L\bar{\rho} \quad (24)$$

$$\int_0^L \rho_n(x) + \rho_{-n}(x) dx = 0, \quad \forall n \neq 0 \quad (25)$$

In the long-time limit, in which the initial conditions have relaxed, integrating over a time period removes any time dependence and leads to the steady time-averaged density probability and flux. Using the expression of the current $j(x, t) = -[D\partial_x\rho(x, t) - D\beta\rho(x, t)f(x, t)]$, we obtain :

$$0 = \frac{1}{T} \int_{t_0}^{t_0+T} \partial_x j(x, t) dt \quad (26)$$

From this expression, one obtains

$$J = \frac{1}{T} \int_{t_0}^{t_0+T} j(x, t) dt \quad (27)$$

$$= -D \left[\partial_x \rho_0(x) - \sum_{n=-\infty}^{\infty} \beta \rho_n(x) f_{-n}(x) \right] \quad (28)$$

Notice that for 1D systems at steady state, J does not depend on position. Using the real nature of both ρ and f , we obtain:

$$J = -D[\partial_x \rho_0(x) - \beta \rho_0(x) f_0(x) - 2 \sum_{n=1}^{\infty} \beta [\operatorname{Re}(\rho_n(x)) \operatorname{Re}(f_n(x)) + \operatorname{Im}(\rho_n(x)) \operatorname{Im}(f_n(x))]] \quad (29)$$

Since J does not depend on space, we can integrate it in x to obtain

$$J = -\frac{D}{L} \int_0^L [\partial_x \rho_0(x) - \beta \rho_0(x) f_0(x) - 2D \sum_{n=1}^{\infty} \beta [\operatorname{Re}(\rho_n(x)) \operatorname{Re}(f_n(x)) + \operatorname{Im}(\rho_n(x)) \operatorname{Im}(f_n(x))]] dx \quad (30)$$

which due to the periodic boundary conditions reads:

$$J = \frac{D}{L} \int_0^L \beta \rho_0(x) f_0(x) + 2 \sum_{n=1}^{\infty} \beta [\operatorname{Re}(\rho_n(x)) \operatorname{Re}(f_n(x)) + \operatorname{Im}(\rho_n(x)) \operatorname{Im}(f_n(x))] dx \quad (31)$$

Using now Eqs. (17), the last expression can be rewritten as

$$J = \frac{D}{L} \int_0^L \beta \rho_0(x) f_0(x) + 2 \sum_{n=1}^{\infty} \beta \operatorname{Re}(\rho_n(x) f_n^*(x)) dx \quad (32)$$

To simplify the calculation, and without loss of generality, we choose

$$\operatorname{Im}(f_i(x)) = 0 \quad (33)$$

Accordingly, using

$$\rho_n(x) = \operatorname{Re}(\rho_n(x)) + i \operatorname{Im}(\rho_n(x)) \equiv R_n(x) + i I_n(x) \quad (34)$$

Eq.(19) can be rewritten as:

$$\begin{aligned} \omega_p R_p(x) &= D \partial_x \left[\partial_x I_p(x) - \sum_n \beta I_n f_{p-n}(x) \right] \\ \omega_p I_p(x) &= -D \partial_x \left[\partial_x R_p(x) - \sum_n \beta R_n f_{p-n}(x) \right] \end{aligned} \quad (35)$$

from which we get:

$$I_p(x) = -\frac{D}{\omega_p} \partial_x \left[\partial_x R_p(x) - \sum_n \beta R_n(x) f_{p-n}(x) \right] \quad (36)$$

and

$$\begin{aligned} \omega_p^2 R_p(x) &= -D^2 [\partial_x^4 R_p(x) - 2 \partial_x^3 \sum_n \beta R_n(x) f_{p-n}(x) \\ &\quad + \beta \partial_x \sum_n [R_n(x) \partial_x^2 f_{p-n}(x) \\ &\quad + 2(\partial_x R_n(x))(\partial_x f_{p-n}(x))] \\ &\quad + \partial_x \sum_n \beta^2 \sum_m f_{p-n}(x) \partial_x (R_m(x) f_{n-m}(x))] \end{aligned} \quad (37)$$

Eq. (37) is a fourth order ODE with non-constant coefficients. In order to get an analytical solution, we assume that the force is homogeneous:

$$f_0(x) = \bar{f}_0 \quad (38)$$

and that the amplitude of the higher modes, f_q is small as compared to f_0 i.e., $f_q \ll f_0 \forall q$. Under these assumptions, we can expand the equation for small values of f_q . The zeroth order of Eq. (37) then reads:

$$\omega_p^2 R_p^{(0)}(x) = -D^2 [\partial_x^4 R_p^{(0)}(x) - 2\beta f_0 \partial_x^3 R_p^{(0)}(x) + \beta^2 f_0^2 \partial_x^2 R_p^{(0)}(x)] \quad (39)$$

whose solution is:

$$R_0^{(0)} = \bar{\rho} \quad (40)$$

$$R_p^{(0)} = 0 \quad \forall p \neq 0 \quad (41)$$

At first order, we have

$$\begin{aligned}\omega_p^2 R_p^{(1)}(x) &= -D^2[\partial_x^4 R_p^{(1)}(x) \\ &\quad - 2\beta\partial_x^3[f_0 R_p^{(1)}(x) + \bar{\rho}f_p(x)] \\ &\quad + \beta\bar{\rho}\partial_x^3 f_p(x) + \beta^2 f_0 \bar{\rho}\partial_x^2 f_p(x)]\end{aligned}\quad (42)$$

We then use the space-Fourier representation

$$R_p^{(1)}(x) = \sum_n R_{p,n}^{(1)} e^{\iota k_n x} \quad (43)$$

$$f_p(x) = \sum_n f_{p,n} e^{\iota k_n x} \quad (44)$$

After projecting onto the mode $n = v$, Eq. (37) reads:

$$\begin{aligned}\left(\frac{\omega_p}{Dk_v^2}\right)^2 R_{p,v}^{(1)} &= -[R_{p,v}^{(1)} + \iota\left(\bar{\rho}\frac{\beta f_{p,v}}{k_v} + 2\frac{\beta f_0}{k_v} R_{p,v}^{(1)}\right) \\ &\quad - \frac{\beta f_0}{k_v}\left(\bar{\rho}\frac{\beta f_{p,v}}{k_v} + \frac{\beta f_0}{k_v} R_{p,v}^{(1)}\right)]\end{aligned}\quad (45)$$

whose solution is:

$$R_{p,v}^{(1)} = -\frac{\beta f_{p,v}}{k_v} \bar{\rho} \frac{\iota - \frac{\beta f_0}{k_v}}{\Gamma_{p,v} + 2\iota \frac{\beta f_0}{k_v}} \quad (46)$$

$$\Gamma_{p,v} = \left(\frac{\omega_p}{Dk_v^2}\right)^2 + 1 - \left(\beta \frac{f_0}{k_v}\right)^2 \quad (47)$$

The second order gives:

$$\begin{aligned}-\frac{\omega_p^2}{D^2} R_p^{(2)}(x) &= \partial_x^4 R_p^{(2)}(x) \\ &\quad - \beta\partial_x^3 [R_p^{(2)}(x)\bar{f}_0 + \sum_{n \neq p} R_n^{(1)}(x)f_{p-n}(x)] \\ &\quad + \beta\partial_x \sum_{n \neq p} [R_n^{(1)}(x)\partial_x^2 f_{p-n}(x) \\ &\quad + 2(\partial_x R_n^{(1)}(x))(\partial_x f_{p-n}(x))] \\ &\quad + \beta^2 \bar{\rho} \sum_{n \neq p} \sum_{m \neq p} \partial_x [f_{p-n}(x)\partial_x f_{n-m}(x)] \\ &\quad + \beta^2 \bar{f}_0 \partial_x [\sum_{n \neq p} f_{p-n}(x)\partial_x R_n^{(1)}(x) \\ &\quad + \sum_{m \neq p} \partial_x (f_{p-m}(x)R_m^{(1)}(x))] \\ &\quad + \beta^2 \bar{f}_0^2 \partial_x^2 R_p^{(2)}(x)\end{aligned}\quad (48)$$

Using

$$R_p^{(2)}(x) = \sum_i R_{p,i}^{(2)} e^{\iota k_i x} \quad (49)$$

once projected, Eq. 48 becomes

$$\begin{aligned}-\frac{\omega_p^2}{D^2} R_{p,v}^{(2)} &= k_v^4 R_{p,v}^{(2)} \\ &\quad + 2\iota\beta \sum_{n \neq p} \sum_i (k_i + k_{v-i})^3 R_{n,i}^{(1)} f_{p-n,v-i} \\ &\quad + 2\iota\beta \bar{f}_0 k_v^3 R_{p,v}^{(2)} \\ &\quad - \iota\beta \sum_{n \neq p} \sum_i [k_{v-i}^2 (k_i + k_{v-i}) R_{n,i}^{(1)} f_{p-n,v-i} \\ &\quad - 2k_i k_{v-i} (k_i + k_{v-i}) R_{n,i}^{(1)} f_{p-n,v-i}] \\ &\quad - \beta^2 \bar{\rho} \sum_{n \neq p} \sum_{m \neq p} [\sum_i k_{v-i} (k_i + k_{v-i}) f_{p-n,i} f_{n-m,v-i}] \\ &\quad - \beta^2 \bar{f}_0 [2 \sum_{n \neq p} \sum_i k_i (k_i + k_{v-i}) f_{p-n,v-i} R_{n,i}^{(1)} \\ &\quad + \sum_{m \neq p} \sum_i k_{v-i} (k_i + k_{v-i}) f_{p-m,v-i} R_{m,i}^{(1)}] - \beta^2 \bar{f}_0^2 k_v^2 R_{p,v}^{(2)}\end{aligned}$$

whose solution, using $k_i + k_{v-i} = k_v$ and dividing by k_v^4 , reads

$$\begin{aligned}R_{p,v}^{(2)} &= \\ &\quad - \frac{\sum_{n \neq p} \sum_i R_{n,i}^{(1)} \frac{\beta f_{p-n,v-i}}{k_v} \left[2\iota - \iota \frac{k_{v-i}}{k_v} \frac{k_{v-i} - 2k_i}{k_v} - 3\left(\frac{\beta \bar{f}_0}{k_v}\right)^2\right]}{\Gamma_{p,v} + 2\iota \frac{\beta \bar{f}_0}{k_v}}\end{aligned}\quad (50)$$

where $\Gamma_{p,v}$ has been defined in Eq. (47).

Finally, we compute the flux at different orders of the expansion.

1. At zeroth order Eq. (32) reads:

$$J^{(0)} = \beta D \bar{\rho} \bar{f}_0 \quad (51)$$

2. At first order, Eq. (32) is:

$$\begin{aligned}J^{(1)} &= 2\frac{\beta D}{L} \sum_p \sum_v \bar{\rho} \beta^2 (\text{Re}(f_{p,v})^2 + \text{Im}(f_{p,v})^2) \\ &\quad \left(\frac{\beta \bar{f}_0}{k_v^2} \frac{\Gamma_{p,v} - 1}{\Gamma_{p,v}^2 + 4\left(\frac{\beta f_0}{k_v}\right)^2}\right)\end{aligned}\quad (52)$$

Introducing the amplitude of the mode $f_{p,v}$

$$|f_{p,v}|^2 \equiv \text{Re}(f_{p,v})^2 + \text{Im}(f_{p,v})^2 \quad (53)$$

the last expression reads:

$$J^{(1)} = 2\frac{\beta D}{L} \sum_p \sum_v \bar{\rho} \beta^2 |f_{p,v}|^2 \frac{\beta \bar{f}_0}{k_v^2} \frac{\Gamma_{p,v} - 1}{\Gamma_{p,v}^2 + 4\left(\frac{\beta f_0}{k_v}\right)^2} \quad (54)$$

which corresponds to Eq.3 of the main text.

which can be identified with Eq.5 of the main text.

3. At second order Eq. 32 reads:

$$J^{(2)} = 2 \frac{\beta D}{L} \sum_p \sum_v \text{Re}(R_{p,v}^{(2)} f_{p,v}^*) \quad (55)$$

-
- [1] S. Perkina and J. Kleinb, *Soft Matter* **9**, 10438 (2013).
- [2] E. Lin, C. Parrish and R. Composto, *Macromolecules* **49**, 5755 (2016).
- [3] K. H. Jensen, K. Berg-Sørensen, H. Bruus, N. M. Holbrook, J. Liesche, A. Schulz, M. A. Zwieniecki, and T. Bohr, *Rev. Mod. Phys.* **88**, 035007 (2016).
- [4] W. Reisner, J. N. Pedersen, and R. H. Austin, *Rep. Prog. Phys.* **75**, 106601 (2012).
- [5] V. Palyulin, T. Ala-Nissila, and R. Metzler, *Soft Matter* **45**, 9016 (2014).
- [6] B. Alberts, A. Johnson, J. Lewis, M. Raff, K. Roberts, and P. Walter, *Molecular Biology of the Cell* (Garland Science, Oxford, 2007).
- [7] L. Bocquet and E. Charlaix, *Chem. Soc. Rev.* **39**, 1073 (2010).
- [8] D. Brogioli, *Phys. Rev. Lett.* **103**, 058501 (2009).
- [9] S.-H. Wu, N. Huang, E. Jaquay, and M. L. Povinelli, *Nano Lett.* **16**, 5261 (2016).
- [10] O. Graydon, *Nature Photon* **11** (2017).
- [11] A. V. Arzola, M. Villasante-Barahona, K. Volke-Sepúlveda, P. Jákl, and P. Zemánek, *Phys. Rev. Lett.* **118**, 138002 (2017).
- [12] J. Brox, P. Kiefer, M. Bujak, T. Schaetz, and H. Landa, *Phys. Rev. Lett.* **119**, 153602 (2017).
- [13] R. Ralph L. Stoop, A. Straube, and P. Tierno, *Nano Lett.* **19**, 433 (2019).
- [14] J. Abbott, A. Straube, D. Aarts, and R. P. A. Dullens, *New J. Phys.* **21** (2019).
- [15] H. Wang, H. W. de Haan, and G. W. Slater, *Electrophoresis* (2019).
- [16] P. Balenzuela, H. Braun, and D. Chialvo, *Contemporary Physics* **53**, 17 (2012).
- [17] P. Zemánek, G. Volpe, A. Jonáš, and O. Brzobohatý, *Adv. Opt. Photon.* **11**, 577 (2019).
- [18] R. Ralph L. Stoop, A. Straube, and P. Tierno, *J. Phys. Chem. C* **123**, 22050 (2019).
- [19] R. L. Stoop, A. V. Straube, and P. Tierno, *Nano Lett.* **19** (2019).
- [20] N. Cohen and J. Boyle, *Contemporary Physics* **51**, 103 (2010).
- [21] *European Journal of Pharmaceutics and Biopharmaceutics* **116**, 125 (2017).
- [22] F. K. Bäuerle, S. Karpitschka, and K. Alim, *Phys. Rev. Lett* **124**, 098102 (2020).
- [23] A. H. Shapiro, M. Y. Jaffrin, and S. L. Weinberg, *J. Fluid Mech.* **37**, 799 (1969).
- [24] M. Li and J. G. Brasseur, *J. Fluid Mech.* **248**, 129 (1993).
- [25] M. Carusela and J. Rubi, *J. Chem. Phys.* **146**, 184901 (2017).
- [26] J. A. Cohen, A. Chaudhuri, and R. Golestanian, *Phys. Rev. Lett.* **107**, 238102 (2011).
- [27] T. Ikonen, J. Shin, W. Sung, and T. Ala-Nissila, *J. Chem. Phys.* **136**, 205104 (2012).
- [28] J. Sarabadani, T. Ikonen, and T. Ala-Nissila, *J. Chem. Phys.* **143**, 074905 (2015).
- [29] D. Mondal and M. Muthukumar, *J. Chem. Phys.* **144**, 144901 (2016).
- [30] T. Menais, S. Mossa, and A. Buhot, *Scientific Reports* **6**, 38558 (2016).
- [31] F. Cecconi, M. A. Shahzad, U. Marini Bettolo Marconi, and A. Vulpiani, *Phys. Chem. Chem. Phys.* **19**, 11260 (2017).
- [32] P. Xu and Y. Jin, *Physica A* **492**, 1281 (2018).
- [33] A. Dubey and M. Bandyopadhyay, *EPJ B* **92**, 251 (2019).
- [34] L. Du, R. Han, J. Jiang, and W. Guo, *Phys. Rev. E* **102**, 012149 (2020).
- [35] S. Marbach, N. Kavokine, and L. Bocquet, *J. Chem. Phys.* **152**, 054704 (2020).
- [36] S. Marbach and K. Alim, *Phys. Rev. Fluids* **4**, 114202 (2019).
- [37] R. L. Westra, *Phys. Rev. E* **100**, 062410 (2019).
- [38] C. Murray, H. Miwa, M. Dhar, D. E. Park, E. Pao, J. Martinez, S. Kaanumale, E. Loghini, J. Graf, K. Rhaddassi, W. W. Kwok, D. Hafler, C. Puleo, and D. Di Carlo, *Lab Chip* **18**, 2396 (2018).
- [39] Q. Guo, S. Duffy, K. Matthews, I. Kerry, M. Emel, and H. Ma, *Scientific Reports* **7**, 6627 (2017).
- [40] R. Di Leonardo, L. Angelani, D. Dell Arciprete, G. Ruocco, V. Iebba, S. Schippa, M. P. Conte, F. Mecarini, F. De Angelis, and E. Di Fabrizio, *Proc. Natl. Acad. Sci.* **107** (2010).
- [41] V. Bianco and P. Magaretti, *J. Chem. Phys.* **145**, 114904 (2016).
- [42] R. Zwanzig, *The Journal of Physical Chemistry* **96**, 3926 (1992).
- [43] D. Reguera and J. M. Rubi, *Phys. Rev. E* **64**, 061106 (2001).
- [44] P. S. Burada, G. Schmid, D. Reguera, J. M. Rubi, and P. Hänggi, *Phys. Rev. E* **75**, 051111 (2007).
- [45] P. Magaretti, I. Pagonabarraga, and M. Rubi, *Frontiers in Physics* **1**, 21 (2013).
- [46] P. Magaretti and J. Harting, *Soft Matter*, in press (2021).
- [47] A. D. Dinsmore and A. G. Yodh, *Langmuir* **15**, 314 (1999).
- [48] J. S. Leith, A. Kamanzi, D. Sean, D. Berard, A. C. Guthrie, C. M. J. McFaul, G. W. Slater, H. W. de Haan, and S. R. Leslie, *Macromolecules* **49**, 9266 (2016).
- [49] The dynamics of the polymer can be mapped onto that of a point-like particle with the effective free energy $\beta A(x, t)$, provided that the relaxation time scale of the polymer, $\tau = 2R_G^2/\pi^2 D$, is much faster than any other time scale.
- [50] O. Kedem, B. Lau, and E. A. Weiss, *Nano Lett.* **17**, 5848 (2017).
- [51] F. K. Bäuerle, S. Karpitschka, and K. Alim, *Phys. Rev.*

Lett. **124**, 098102 (2020).